Applied Catalysis B: Environmental 99 (2010) 145–155

Contents lists available at ScienceDirect

Applied Catalysis B: Environmental

journal homepage: www.elsevier.com/locate/apcatb

A kinetic study of the reduction of NO_x stored on Pt-Ba/Al_2O_3 catalyst

P. Forzatti, L. Lietti*, N. Gabrielli

Laboratory of Catalysis and Catalytic Processes and NEMAS Centre of Excellence, Dipartimento di Energia, Politecnico di Milano, Piazza Leonardo da Vinci, 32, 20133 Milano, Italy

ARTICLE INFO

Article history:
Received 1 March 2010
Received in revised form 28 May 2010
Accepted 7 June 2010
Available online 11 June 2010

Keywords:
NO_x reduction
Pt-Ba/Al_2O_3
NO_x Trap
Kinetics
Hydrogen
Ammonia
Spatiotemporal resolution

ABSTRACT

A kinetic study for the reduction of NO_x stored onto a Pt-Ba/Al_2O_3 LNT catalyst is developed, based on previous experimental work where regeneration of stored NO_x was accomplished under isothermal wet conditions using ammonia and hydrogen as reducing agents [L. Lietti, I. Nova, P. Forzatti, J. Catal. 257 (2008) 270–282]. The kinetic model developed in the present paper differs from those available in the literature because it considers the most relevant physico-chemical features of regeneration of LNT catalysts under nearly isothermal conditions. It is based exclusively on a consecutive reaction scheme with ammonia as intermediate, as proposed in the previous study, and on a mechanism which considers only surface reactions of stored NO_x. The model includes the elementary-like steps of adsorption–desorption of hydrogen, ammonia and water at Pt sites, and the lumped steps of reduction of stored nitrates by hydrogen to give ammonia and of reduction of residual stored nitrates by ammonia to give nitrogen. A surface dependent energy of activation for the reduction of nitrates with ammonia is required to describe the data in the T interval 150–300 °C. This is due to the presence of nitrates with high and low reactivity that are envisaged as close and far from the noble metal crystallites, respectively. A low energy of activation (22.94 kJ/mol) is estimated for the reduction of nitrates by hydrogen to give ammonia. This applies above a consumption of $1.5–2 \times 10^{-4}$ mol of stored NO_x/g_{cat}, where the residual NO_x species are expectedly stored far from the Pt crystallites and the rate of their consumption is limited by surface diffusion. Before this consumption level the reaction is limited by the concentration of hydrogen at any temperature in the T interval 150–350 °C. The model is shown to capture the major features of the isothermal experiments performed under wet conditions over Pt-BaO/Al_2O_3 LNT catalyst with hydrogen and ammonia as reducing agents in the T interval 150–350 °C and is able to describe nicely on a purely predictive basis independent NH_3-TPSR experiments. However the model underestimates H_2 consumption and net NH_3 production during independent H_2-TPSR experiments below 100 °C, where the consumption of stored NO_x is less than 1×10^{-4} mol/g_{cat} and is associated with fast regeneration of Ba sites in close proximity to the Pt crystallites. The model is also used to simulate the axial concentration profiles in the reactor for gas and surface species as function of time during regeneration with ammonia.

1. Introduction

NO_x storage-reduction (NSR) is a promising technology for meeting upcoming stringent regulations on NO_x emission in particular from light duty diesel engines and lean burn gasoline engines [2,3]. The operation of NSR catalysts (also quoted as Lean NO_x Trap, LNT) comprises a long lean period in which the NO_x emitted in the exhaust gases are adsorbed on the catalyst surface in the form of nitrites and nitrates and a short fuel-rich period in which the stored NO_x are reduced by H_2, CO and unburned hydrocarbons to give N_2. The LNT catalysts typically consist of a NO_x storage component such as Ba or K, and of a noble metal such as Pt that catalyses the oxidation of NO and the combustion of CO and unburned hydrocarbons during the lean period and the reduction of stored NO_x during the rich period; these catalysts components are dispersed on high surface area alumina support. The commercial LNT catalysts can also contain other components such as Ce for oxygen storage capacity (OSC) and other noble metals (e.g. Rh) to catalyse the WGSR and the reforming of hydrocarbons.

Ammonia formation and reaction over NSR catalysts during regeneration has been observed and studied [1,4–18]. Castoldi et al. [6] and Nova et al. [9] report catalyst effluent NH_3 slip at the end of regeneration of stored NO_x by hydrogen over a Pt-Ba/Al_2O_3 sample; they speculated that regeneration of nitrates in close proximity to Pt (fast NO_x storage/reduction sites) might account for the production of nitrogen while nitrates less proximal to Pt (slow NO_x storage/reduction sites) are regenerated later to give ammonia. The importance of coupling between the precious metal and BaO where storage of NO_x takes place was first addressed by Mazhoul et al. [19]. Pihl et al. [8] found that ammonia formation is favoured at

* Corresponding author. Tel.: +39 02 2399 3272, fax: +39 02 7063 8173.
E-mail address: luca.lietti@polimi.it (L. Lietti).

0926-3373/$ – see front matter © 2010 Elsevier B.V. All rights reserved.
doi:10.1016/j.apcatb.2010.06.011

Nomenclature

a	unit cell dimension of the FCC structure
$\underline{b}$	vector of the adaptive parameters of the kinetic model
C	concentration of gaseous species (mol/m^3)
$D_{Pt\,cryst}$	diameter of the Pt crystallite
E	activation energy
E_{MIN}	minimum value of the energy of activation E_{S5}
E_{MAX}	maximum value of the energy of activation E_{S5}
k^0	pre-exponential kinetic constant
L	reactor length
M	molecular weight
N_{Av}	Avogadro number
N_{NO_x}	number of moles of NO_x
$N_{Pt\,cryst}$	number of Pt crystallites
$N_{Pt\,at}$	number of Pt atoms
NS	number of species i involved in the reduction
Nt	number of experimental data as function of time at a given T
$P_{Pt\,cryst}$	total perimeter of the Pt crystallites
R	gas constant
R_i	reaction rate of step i or net rate of production/consumption of species i
S_i	step i
S_0	sticking coefficient at 0 coverage
t	time
T	temperature
x_w	weight fraction
y_i	experimental value of kinetic datum i
y_i^{mod}	model prediction of kinetic datum i
z	reactor axial coordinate
Z	number of molecules in the unit cell

Greek letters

$\Omega_{Ba(NO_3)_2}$	NO_x adsorption capacity of the catalyst associated with Ba sites
Ω_{Pt}	Pt catalyst capacity
α	adaptive parameter in E_{S5}
α_V	catalyst active Pt surface area
β	kinetic parameter after re-parameterization
ε	reactor void fraction
γ	adaptive parameter in E_{S5}
θ_i	fractional coverage of surface species i
τ	residence time
ω_i	weight associated to species i

Subscripts

act	active
ads	adsorption
at	atom
cryst	crystallite
des	desorption
i	index of gaseous and surface component
j	index of the reaction step
tot	total

high ratios of the reducing agent to NO_x and lower temperatures; they noted that ammonia formed in one portion of the catalyst could be consumed in another portion of the catalyst via regeneration reactions or reduction of stored oxygen and emphasised the importance of slow sites. Ribeiro and co-workers [10,11] suggested that the regeneration of Pt-Ba/Al_2O_3 monolith NO_x Trap with hydrogen occurs through a complex pathway where at first nitrogen and ammonia can be formed according to a parallel scheme via recombination of surface Pt-N species produced from dissociative adsorption of gaseous NO at metal Pt and via successive recombination of Pt-N and Pt-H species, respectively. However the selective catalytic reduction of NO_x with ammonia and the oxidation of ammonia to give nitrogen are also considered in their scheme. Both Pihl et al. [8] and Ribeiro and co-workers [11] emphasise in their models the integral nature of the NO_x Trap during regeneration so that a plug flow regeneration front and the associated concentration fronts of reactants and products develop, which travel along the reactor axis. They also assume the release of NO_x from the trapping material in the gas phase as the first step in the process and note that it is not necessary to invoke a mechanism of surface diffusion of NO-containing species that are reduced at Pt. On the opposite Nova et al. [17] and Forzatti and Lietti [18] have shown that both H_2 and NH_3 can directly regenerate NO_x stored onto Pt-Ba/Al_2O_3 under nearly isothermal conditions via a Pt catalysed reaction that does not involve gaseous NO; they also suggest a two-steps reaction pathway involving the fast reaction of H_2 with stored NO_x to give ammonia and the subsequent slower reaction of ammonia with stored NO_x to give N_2. Recently Lietti et al. [1,14] proposed that N_2 is formed exclusively via this in series two-steps pathway and also showed that the reduction of stored NO_x with H_2 to give ammonia is much faster in the presence of water. The papers cited above convey a complex network of reactions of ammonia formation and utilisation in different zones of the reactor, where release of stored NO_x to give NO/NO_2 in the gas phase and surface diffusion of NO-containing species are either assumed or disregarded.

In recent papers effluent measurements of different length catalyst sections [15] and intra catalyst measurements using spatially resolved inlet mass spectrometry (SpaciMS) [16] have been used to obtain a spatiotemporal resolution during Pt-Ba/Al_2O_3 monolith LNT regeneration. On the other hand regeneration of stored NO_x using a limited concentration of the reducing agent and with a purge of inert gas (e.g. He) in between the lean and the rich periods has been used in the laboratory to attain nearly isothermal conditions that prevent the thermal release of NO_x in the gas phase and the associated greater complexity of network of reactions and to ensure a complete decoupling of storage and reduction chemistry [1,13,17].

A number of kinetic models of varying complexity have been developed in the literature to describe the regeneration of NO_x Traps.

A detailed microkinetic model of NO_x storage and reduction has been presented by Olsson et al. [20,21]. The model could describe NO_x storage and regeneration with propene. The same group at Chalmers, in cooperation with the group at Cummins, has recently developed a detailed microkinetic model that describes NO_x storage (NO_x is allowed to be stored at two different types of sites) and reduction with H_2 in the presence of H_2O and CO_2 over Pt-Ba/Al_2O_3 monolith sample and also considers ammonia formation and consumption [22]. In this model the release at first of stored NO_x in the gas phase is assumed to account for the NO_x spike observed immediately upon switch from lean to rich conditions in commercial operation. Nitrogen is formed by reaction of two Pt-N species produced by NO decomposition at Pt sites and ammonia is formed by the reaction of P-N with Pt-H species, the last ones produced by dissociative adsorption of hydrogen. Ammonia is consumed to give N_2 by oxidation over Pt and by surface reaction with Ba nitrates and Ba nitrites. The parameters in the model are derived from kinetic gas theory, transition state theory, statistical thermodynamics, thermodynamic constraints, literature, experiments or are fitted to the experiments using least square methods. Microkinetic models were also developed by Xu et al. [23] and by Larson et al. [24] for the NO/H_2 gaseous reaction system using a commer-

cial monolith NO_x Trap catalyst. This model is relevant to real LNT operation under non-isothermal conditions where thermal decomposition of stored NO_x is observed upon switch from lean to rich conditions. The model includes NO decomposition to N_2O and N_2, hydrogen reduction of adsorbed oxygen and OH groups to H_2O, and the hydrogenation of N ad-atoms to NH_3. In both these studies N_2 was not directly measured and was calculated assuming an instantaneous N atomic balance.

Koci and co-workers [25,26] developed a spatially distributed NSR model based on global kinetics for an industrial NSR catalyst of NM-Ba-CeO_2/Al_2O_3 type (NM: noble metal) involving rate expressions that include only gas-phase concentrations. The model of Koci et al. considered at first only the reduction of NO_x by CO, H_2 and unburned hydrocarbons but was later extended to include the formation of NH_3 by reaction of H_2 with nitrates and the subsequent reaction of ammonia with oxygen, with NO_x adsorbed on the catalyst surface and with NO from the gas phase, producing N_2. Reaction kinetic parameters have been evaluated from a series of laboratory experiments collected over an industrial monolith sample and the model was validated over test bench measurements at Daimler. Global kinetic models were also developed by Tuttlies et al. [27], Olsson et al. [28,29], Sharma et al. [30,31] and Sholtz et al. [32] where the solid diffusion described by a shrinking core model and the presence of multiple storage sites are considered but ammonia formation and consumption are not included. Recently a global kinetic model was developed by Cao et al. [33] where it is assumed that the regeneration of the partially saturated monolith Pt-Ba/Al_2O_3 catalyst using H_2 as the reducing agent involves the formation of NH_3 as intermediate from the stored NO_x and that NH_3 acts as carrier of H atoms.

Along similar lines Clayton et al. [15,34] developed a simplified global kinetic model for NO_x storage and reduction with hydrogen over a Pt-Ba/Al_2O_3 monolith catalyst. The model assumes the existence of two different types of BaO sites on the catalyst, which differ in their storage as well as regeneration activity. The fast storage/reduction sites are conjectured to be in close proximity to the Pt/BaO interface, while the slow sites are far from the Pt sites. The reduction scheme considers the formation of ammonia from nitrates and its consumption by stored NO_x to form N_2. The global kinetic model was incorporated into a one-dimensional two phase transient model of the reactor to predict the spatiotemporal concentration profiles measured and the surface coverage calculated over a series of monoliths of progressively decreasing length under near isothermal conditions at a single temperature of 275 °C.

In the present paper regeneration data of LNT Pt-Ba/Al_2O_3 catalyst in the powder form based on previous experimental work [1] are used to derive a kinetic model. Based on the reaction pathway pointed out in [1] and differently from other literature studies, the model is based exclusively on the consecutive reaction scheme with formation of ammonia from nitrates followed by reaction of ammonia with residual nitrates to give nitrogen, and consists of both elementary-like and lumped steps. The regeneration of the LNT Pt-Ba/Al_2O_3 catalyst was accomplished using both H_2 and NH_3 as reducing agents to address the role of ammonia as intermediate in the regeneration with hydrogen. The regeneration was realised both in the presence and absence of water in the feed [1]. Here only the experiments realised in the presence of water are considered because in the absence of water a large induction period was observed that complicates the kinetic description of the reacting system. Finally the regeneration was accomplished under nearly isothermal conditions with limited concentration of H_2 and of NH_3 and with a He purge in between storage and regeneration periods to prevent thermal release of NO_x and transients in the oxygen gas-phase concentration upon the lean-fuel rich switch. This differs from regeneration in commercial NO_x traps where oxygen is present resulting in a significant temperature rise.

Table 1
Catalyst characteristics.

Catalyst composition	BET surface area	Pt dispersion (H/Pt)	Mean dimension of Pt crystallites, D_{cryst}
Pt-Ba/Al_2O_3 (1/20/100 w/w/w)	140 m^2/g	0.55	2.0 nm

We show that the simple description of the regeneration scheme provided by the model is able to describe on a sound and quantitative basis the isothermal experimental data. The reactor model which incorporates the kinetic scheme based exclusively on the in series two steps pathway with ammonia as intermediate is validated against independent NH_3- and H_2-TPSR experiments. The model is also used to provide a spatiotemporal resolution of the LNT reactor during regeneration with ammonia.

2. Model development

2.1. Experimental data

The experiments that were used to develop the kinetic model were carried out in a quartz tubular fixed-bed micro-reactor using 60 mg of a Pt/BaO/γ-Al_2O_3 (1/20/100, w/w/w) LNT catalyst sample in the powder form (100–150 μm) [1]. The catalyst was prepared by successive impregnation of the γ-Al_2O_3 carrier calcined at 700 °C with aqueous solutions of $Ba(CH_3COO)_2$ first and of $Pt(NH_3)_2(NO_2)_2$ next after drying at 80 °C and calcination at 500 °C in between and final calcination at 500 °C for 5 h [1]. The Pt loading is 0.83% (w/w) and the metal dispersion, measured by hydrogen chemisorption at room temperature, is 55%. The BET surface area is around 140 m^2/g and the Ba content of 16.5% (w/w) ensures an almost complete coverage of the alumina surface. The mean particle diameter of the Pt crystallites, calculated from Pt dispersion using the empirical relationship D_{cryst} (nm) = 1.1/(H/Pt) [35], is 2.0 nm, which compares well with that measured by HRTEM for another preparation batch of a catalyst with the same composition [36]. The characteristics of the catalyst are summarised in Table 1.

After catalyst conditioning, realised by performing few adsorption/regeneration cycles with NO/O_2 (1000 ppm NO and 3% (v/v) O_2 in He) and H_2 (2000 ppm in He) at 350 °C with an inert purge (He) between the two phases, NO_x were adsorbed at the same temperature of 350 °C. The NO_x storage was accomplished by imposing a rectangular step feed of NO (1000 ppm) in flowing He + 3% (v/v) O_2 for about 400 s, followed by a He purge to provoke the desorption of weakly adsorbed species. The temperature of 350 °C and the duration of the storage phase guarantee that at the beginning of the regeneration phase stored NO_x are present primarily in the form of nitrates [18], as also revealed by FTIR experiments [37], and that the surface coverage of nitrates is close to saturation and it can be assumed as almost constant along the axis of the reactor.

In the experiments used to develop the kinetic model the reduction of NO_x stored at 350 °C was accomplished at four T values between 150 and 350 °C. During He purge after NO_x adsorption at 350 °C the catalyst temperature was set to the desired level and then, after stabilisation of the Mass Spec signals, H_2 (2000 ppm in He + 1% H_2O, v/v) or NH_3 (1000 ppm in He + 1% H_2O, v/v) were admitted in a step-wise manner. A complete decoupling of the storage and of the reduction phases was achieved by applying an He purge in between the two phases. Besides, the transients in the oxygen gas-phase concentration upon the lean-rich switch, with the associated undesired reactions of complete oxidation, were avoided. Moreover isothermal conditions were realised in the catalyst bed, due to the small concentration of H_2 or NH_3 employed during regeneration. Accordingly the thermal decomposition of

surface nitrates was prevented and the chemistry of Pt catalysed NO_x/H_2 and NO_x/NH_3 gas mixtures could be neglected in the kinetic scheme with a significant simplification of the reaction network. Then, when the reduction process was completed, the H_2 and NH_3 flow was stopped, the catalyst was heated at 350 °C under He atmosphere and the amounts of residual stored NO_x was then estimated by reduction at this temperature with H_2 or with NH_3, respectively.

Different TPSR experiments were used for the validation of the kinetic model. In these experiments after storage at 350 °C and cooling in He down to room temperature the reduction of stored NO_x was accomplished under a reducing atmosphere (2000 ppm H_2 in He + 1% H_2O, v/v, 1000 ppm H_2 in He + 1% H_2O, v/v, 2200 ppm NH_3 in He + 1% H_2O, v/v and 550 ppm NH_3 in He + 1% H_2O, v/v) with an heating rate of 10 °C/min up to 500 °C.

Preliminary experiments, where a step-wise change in the feed ammonia concentration (from 0 to 1000 ppm) was applied to the empty micro-reactor (i.e. a reactor with no catalyst but with all else), showed an ammonia "time delay" that was described by NH_3 adsorption–desorption onto the Mass Spec capillary line kept at 90 °C.

2.2. Kinetic model

In this section a kinetic model is developed to describe the reduction of stored nitrates by H_2 and NH_3 in the presence of water. In order to explain the product distribution the following sequence of steps is considered:

S1: $2Pt + H_2 \leftrightarrow 2Pt\text{-}H$
S2: $Pt + NH_3 \leftrightarrow Pt\text{-}NH_3$
S3: $Pt + H_2O \leftrightarrow Pt\text{-}H_2O$
S4: $Ba(NO_3)_2 + 16Pt\text{-}H \rightarrow 2NH_3 + BaO + 5H_2O + 16Pt$
S5: $3Ba(NO_3)_2 + 10Pt\text{-}NH_3 \rightarrow 8N_2 + 3BaO + 15H_2O + 10Pt$

Elementary-like steps S1–S3 describe the adsorption–desorption of hydrogen, ammonia and water at Pt site respectively. Steps S4 and S5 describe in a lumped manner the reduction of stored nitrates by hydrogen to give ammonia and the reduction of stored nitrates by ammonia to give nitrogen respectively, and account for the products observed in the reaction system. Notice that BaO in steps S4 and S5 can be transformed in the presence of water into $Ba(OH)_2$ according to the reaction: $BaO + H_2O \rightarrow Ba(OH)_2$.

The reduction either by hydrogen or by ammonia of Pt-O remaining on the catalyst surface after lean NO_x storage followed by He purge is neglected. Indeed the amount of PtO sites is small relative to the consumption of reductants via the other reactions. Besides this reaction is considered to be very fast at any temperature, so that it is completed in less then 10 s. Accordingly it does not affect to any significant extent the dynamics of the reduction process.

The rate expressions for each step are given in Table 2. The kinetic parameters in the rate equation of adsorption of species i in step j are given by:

$$k_{\mathrm{ads},j} = S_{i,0}(2\pi M_i/T/R)^{0.5} \times \alpha_V$$

Table 2
Rate expressions for each of the steps of the kinetic model.

Reaction step j	Rate expression
S1	$R_{S1} = k_{\mathrm{ad},H_2} \times \theta_{Pt}^2 \times C_{H_2} - k_{\mathrm{des},H_2} \times \theta_{Pt\text{-}H^2}$
S2	$R_{S2} = k_{\mathrm{ads},NH_3} \times \theta_{Pt} \times C_{NH_3} - k_{\mathrm{des},NH_3} \times \theta_{Pt\text{-}NH_3}$
S3	$R_{S3} = k_{\mathrm{ads},H_2O} \times \theta_{Pt} \times C_{H_2O} - k_{\mathrm{des},H_2O} \times \theta_{Pt\text{-}H_2O}$
S4	$R_{S4} = k_4 \times \Omega_{Ba(NO_3)_2}\theta_{Ba(NO_3)_2} \times \theta_{Pt\text{-}H}$
S5	$R_{S5} = k_5 \times \Omega_{Ba(NO_3)_2}\theta_{Ba(NO_3)_2} \times \theta_{Pt\text{-}NH_3}$

$$k_{\mathrm{des},j} = k^0_{\mathrm{des},j} \exp\left(\frac{-E_{\mathrm{des},j}}{RT}\right)$$

with $i = H_2$, NH_3 and H_2O and j = S1, S2, S3. $S_{i,0}$ is the sticking coefficient, M_i the molecular weight of species i, α_V the catalyst active Pt surface area (see Table 1), and R the gas constant. The kinetic constants k_j of the reaction rate of step j = S4, S5 are described by the Arrhenius expression:

$$k_j = k^0_j \exp\left(\frac{-E_j}{RT}\right)$$

where k^0_j and E_j are the corresponding pre-exponential coefficient and the activation energy. The rate expressions for the lumped processes S4 and S5 in Table 2 assume that the first reduction step of nitrates by adsorbed hydrogen (Pt-H) or adsorbed ammonia (Pt-NH_3), respectively is rate determining and accordingly show a first order dependence on the surface concentration of $Ba(NO_3)_2$ ($\Omega_{Ba(NO_3)_2}\theta_{Ba(NO_3)_2}$) and on either $\theta_{Pt\text{-}H}$ and $\theta_{Pt\text{-}NH_3}$. $\Omega_{Ba(NO_3)_2}$ is the NO_x adsorption capacity of the catalyst associated with Ba sites (mol/m^3_{cat}) and θ_i is the fractional coverage of surface species i ($i = Ba(NO_3)_2$, P-H, Pt-NH_3).

The adsorption–desorption of hydrogen, ammonia and water on Pt have been widely studied and the rate constants of steps S1, S2 and S3 were taken from literature and are given in Table 3. The parameter in brackets in Table 3 was not retained in the kinetic study and was estimated by regression to the experimental data of reduction of nitrates with ammonia to help predict certain trends in the experimental data, as also done elsewhere [23].

2.3. Reactor model

The experimental data collected over the powder catalyst were analysed according to a dynamic 1-D isothermal pseudo-homogeneous plug flow model of the laboratory micro-reactor. On the basis of diagnostic criteria the influence of both intra-particle catalyst gradients and external mass transfer limitations were found negligible. Under these hypotheses the unsteady mass balances for gas species (H_2, NH_3, N_2, H_2O) are given below:

$$(H_2)\quad \varepsilon\frac{\partial C_{H_2}}{\partial t} = -\frac{1}{\tau}\frac{\partial C_{H_2}}{\partial z} + (1-\varepsilon)R_{H_2}, \quad R_{H_2} = -R_{S1}$$

$$(NH_3)\quad \varepsilon\frac{\partial C_{NH_3}}{\partial t} = -\frac{1}{\tau}\frac{\partial C_{NH_3}}{\partial z} + (1-\varepsilon)R_{NH_3}, \quad R_{NH_3} = -R_{S2} + 2R_{S4}$$

Table 3
Kinetic parameters taken from the literature.

Step	Sticking coefficient, $S_{i,0}$	Rate constant of adsorption, $k_{\mathrm{ads},i}$ (s^{-1})	Pre-exponential factor, $k^\circ_{\mathrm{des},i}$ (s^{-1})	Desorption energy, $E_{\mathrm{des},i}$ (kJ/mol)	Reference
S1	0.046	1.948×10^4	3.690×10^{21}	67.0	[38]
S2	1	1.331×10^5	$[3.032 \times 10^8]$	48.4	[39]
S3	0.75	9.705×10^4	1.794×10^{14}	40.3	[38]

$$(N_2)\quad \varepsilon\frac{\partial C_{N_2}}{\partial t} = -\frac{1}{\tau}\frac{\partial C_{N_2}}{\partial z} + (1-\varepsilon)R_{N_2}$$
$$R_{N_2} = -8R_{S5}$$

$$(H_2O)\quad \varepsilon\frac{\partial C_{H_2O}}{\partial t} = -\frac{1}{\tau}\frac{\partial C_{H_2O}}{\partial z} + (1-\varepsilon)R_{H_2O}$$
$$R_{H_2O} = -R_{S3} + 5R_{S4} + 15R_{S5}$$

where C_i is the gas phase concentration of species i, R_i the net rate of reaction of species i (i = H_2, N_2, NH_3, H_2O), z the non-dimensional reactor axial coordinate, τ the residence time, ε the reactor void fraction and t is time. The unsteady mass balances for surface species ($Ba(NO_3)_2$, BaO, Pt, Pt-H, Pt-NH_3, Pt-H_2O) are given below:

$$(Ba(NO_3)_2)\quad \Omega_{Ba(NO_3)_2}\frac{\partial\theta_{Ba(NO_3)_2}}{\partial t} = R_{Ba(NO_3)_2}$$
$$R_{Ba(NO_3)_2} = -R_{S4} - 3R_{S5}$$

$$(BaO)\quad \Omega_{Ba(NO_3)_2}\frac{\partial\theta_{BaO}}{\partial t} = R_{BaO}$$
$$R_{BaO} = R_{S4} + 3R_{S5}$$

$$(Pt)\quad \Omega_{Pt}\frac{\partial\theta_{Pt}}{\partial t} = R_{Pt}$$
$$R_{Pt} = -2R_{S1} - R_{S2} - R_{S3} + 16R_{S4} + 10R_{S5}$$

$$(Pt\text{-}H)\quad \Omega_{Pt}\frac{\partial\theta_{Pt\text{-}H}}{\partial t} = R_{Pt\text{-}H}$$
$$R_{Pt\text{-}H} = 2R_{S1} - 16R_{S4}$$

$$(Pt\text{-}NH_3)\quad \Omega_{Pt}\frac{\partial\theta_{Pt\text{-}NH_3}}{\partial t} = R_{Pt\text{-}NH_3}$$
$$R_{Pt\text{-}NH_3} = R_{S2} - 10R_{S5}$$

$$(Pt\text{-}H_2O)\quad \Omega_{Pt}\frac{\partial\theta_{Pt\text{-}H_2O}}{\partial t} = R_{Pt\text{-}H_2O}$$
$$R_{Pt\text{-}H_2O} = R_{S3}$$

$\Omega_{Ba(NO_3)_2}$ has already been defined as the NO_x adsorption capacity of the catalyst associated with Ba sites, Ω_{Pt} is the catalyst Pt surface capacity (mol/m^3_{cat}), θ_i and R_i are the surface coverage and the net rate of reaction of catalyst surface species i (i = BaO, $Ba(NO_3)_2$, Pt, Pt-H, Pt-NH_3, Pt-H_2O), and t is time.

$\Omega_{Ba(NO_3)_2}$ is calculated from the moles of NO_x stored during the lean phase and differs slightly among the set of experiments considered in the present study. The N-balance, estimated by comparing the amounts of NO_x adsorbed during the lean phase with those of the N-containing species formed both on reduction at the investigated temperature and on the final reduction at 350 °C with the same reducing agent (i.e. H_2 or NH_3), always closed within ±5%. Ω_{Pt} was calculated from H_2 chemisorption measurements at room temperature (see Section 2). Accordingly these two parameters were not fitted to the experimental data.

The initial and boundary conditions are specified below and include zero concentration of the reducing agent (either H_2 or NH_3) at time zero at any axial position in the reactor and constant concentration of the same reducing agent at any time at the inlet of the reactor, after the stepwise increase. Also the concentration of water is equal to 1% (v/v) at the entrance of the reactor at any time and is constant along the reactor axis at time zero. Besides the fractional coverage of the surface species along the axial position of the reactor is uniform at time zero.

$$C_i(0,z) = C_{i,t_0}\quad (i = H_2, NH_3, H_2O)$$
$$C_i(t,0) = C_{i,z_0}\quad (i = H_2, NH_3, H_2O)$$
$$\theta_i(0,z) = \theta_{i,t_0}\quad (i = BaO, Ba(NO_3)_2, Pt, Pt\text{-}H, Pt\text{-}NH_3, Pt\text{-}H_2O)$$

The delay of ammonia (see Section 2) is accounted for by a PFR model where NH_3 adsorption–desorption takes place onto the Mass Spec capillary walls at 90 °C (T set of the MS capillary) and in series to the catalytic laboratory micro-reactor. The dynamics of NH_3 adsorption–desorption in the Mass Spec capillary was calculated from preliminary experiments.

The energy balance equations are not incorporated in the model because of the isothermal conditions of the experimental data.

The reactor model consists of 10 PDEs and was solved numerically using the method of lines. The axial reactor length was split into 25 grid points and in each point the spatial derivates were approximated by the Eulero backward differentiation method. Thus from a 10 PDEs problem a 250 grid points ODEs system was obtained and solved using the BzzMath 6.0 library [40].

The four experiments where the reduction of stored NO_x was accomplished with ammonia at constant temperature at 150, 200, 250 and 300 °C were used to estimate the parameters of step S5 and k^0_{des,NH_3}. Then these parameters were fixed to the values of this regression and the other two parameters k^0_4, and E_4 were estimated by regression to the set of four experiments where the reduction of stored NO_x was accomplished with hydrogen at 150, 200, 250 and 350 °C.

The adaptive kinetic parameters were estimated by minimising the weighted residual sum of squares between experimental values and model predictions for the complete data set [41]:

$$\min_{\underline{b}}\sum_{i=1}^{NS}\left(\sum_{j=1}^{Nt}\omega_i\left(y^{exp}_{i,j} - y^{mod}_{i,j}(\underline{b})\right)^2\right)$$

where NS is the number of species (i) involved in the reduction, Nt is the number of experimental data as function of the time, ω_i is the weight associated to species i, $\underline{b}$ is the vector that contain the adaptive parameters of the model.

Re-parameterization was made to reduce the strong correlation between the pre-exponential factor and the activation energy, as given below:

$$\beta^{des,i}_1 = \ln(k^o_{des,i})\quad \beta^j_1 = \ln(k^o_j)$$
$$\beta^{des,i}_2 = \frac{-E_{des,i}}{R}\quad \beta^j_2 = \frac{-E_j}{R}$$
$$k_{des,i} = \exp\left[\beta^{des,i}_1 + \frac{\beta^{des,i}_2}{T}\right]\quad k_j = \exp\left[\beta^j_1 + \frac{\beta^j_2}{T}\right]$$

3. Results and discussion

3.1. Reduction of stored NO_x with NH_3

Fig. 1 shows the experimental concentration of effluent NH_3 and of effluent N_2 at the MS quadrupole detector (open symbols) during the reduction of stored nitrates with ammonia at four different temperatures. At 150 °C (panel A) only a limited consumption of ammonia and a small concentration of nitrogen are measured. At higher temperatures (200 °C in panel B, 250 °C in panel C and 300 °C in panel D) and at the beginning of the regeneration phase the process is always limited by the concentration of the reducing agent and ca 800 ppm of nitrogen are produced. At higher regeneration times a decrease in the effluent nitrogen concentration is observed, which anticipates the ammonia breakthrough due to delay of the effluent ammonia concentration associated with NH_3 adsorption–desorption in the capillary of the Mass Spectrometer.

Table 4
Moles of nitrates stored at 350 °C consumed during the reduction at different temperatures.

Reducing agent	T (°C)	Reduction time (s)	NO_x reduced at given time (mol/gcat)	NO_x reduced at the given T+ at 350 °C (mol/g_{cat})	NO_x reduction efficiency (%)
NH_3	150	1000	3.468×10^{-5}	2.268×10^{-4}	–
		4860	1.313×10^{-4}		58
	200	1000	2.723×10^{-4}	2.989×10^{-4}	–
		1560	2.755×10^{-4}		92
	250	1000	2.921×10^{-4}	2.963×10^{-4}	–
		1430	2.927×10^{-4}		99
	300	1000	2.905×10^{-4}	2.936×10^{-4}	–
		1170	2.909×10^{-4}		99
H_2	150	1000	2.695×10^{-4}	3.082×10^{-4}	–
		1750	3.033×10^{-4}		98
	200	1000	2.875×10^{-4}	3.040×10^{-4}	–
		1480	2.995×10^{-4}		99
	250	1000	3.103×10^{-4}	3.267×10^{-4}	–
		1450	3.252×10^{-4}		100
	350	815	2.818×10^{-4}	2.818×10^{-4}	100

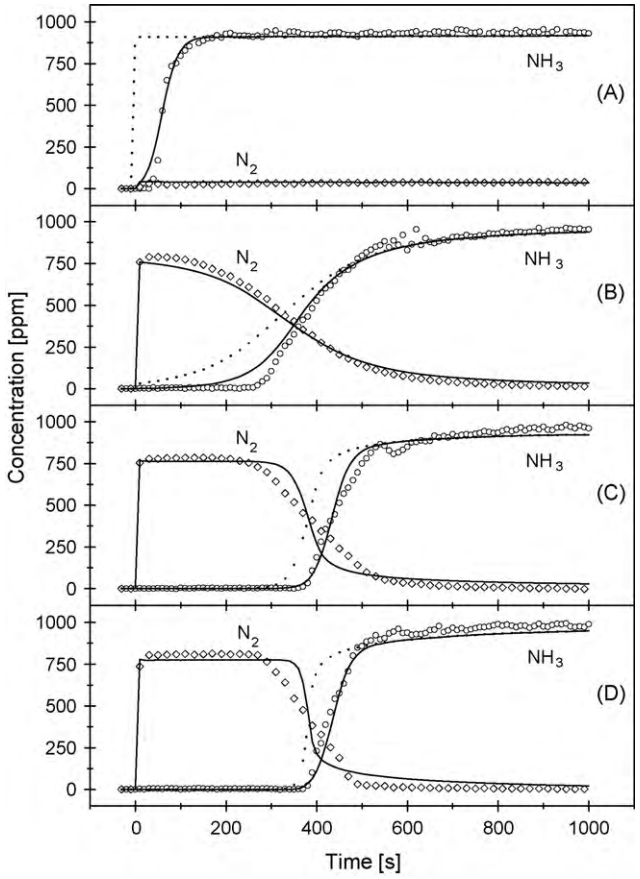

Fig. 1. Isothermal reduction with NH_3 of NO_x stored at 350 °C: (A) T = 150 °C; (B) T = 200 °C; (C) T = 250 °C; (D) T = 300 °C. Experimental concentration of NH_3 and N_2 at the MS detector, open symbols; model prediction of effluent concentration of NH_3 and N_2 at the MS detector, full lines; model prediction of effluent concentration of NH_3 at the reactor exit, dashed line. The inlet concentration of NH_3 is set at 1000 ppm at t = 0.

On increasing the reduction temperature the decrease in nitrogen concentration and the corresponding NH_3 breakthrough curves are observed later and become steeper due to the higher rate of reaction. At the given temperature, as the regeneration proceeds further with time, the concentration of nitrogen drops to zero and the NH_3 concentration approaches the inlet value showing that the reduction process is complete.

From these experiments and the final reduction run accomplished thereafter at 350 °C it is possible to calculate for each temperature the moles of NO_x reduced by NH_3 to form nitrogen (after the time period of 1000 s shown in Fig. 1 and till the end of the experiment) and also the sum of these moles with those that are reduced at 350 °C; these last ones correspond the moles of NO_x previously stored onto the catalyst at 350 °C. These quantities are listed in Table 4. In the same table the reduction efficiency at the end of the isothermal experiment, defined as the ratio between the moles of NO_x reduced at a given temperature to the sum of these moles with those that are reduced thereafter at 350 °C, is also given. The stored NO_x that are involved in the reduction process increase with temperature, particularly in the range 150–200 °C, and the reduction efficiency approaches 100% only at $T \geq 200$ °C. This clearly demonstrates that nitrates with different reactivity are present at the catalyst surface and that less reactive sites take part in the reaction only at $T \geq 200$ °C but not at 150 °C. The more and less reactive nitrates are envisaged as close and far from the noble metal, respectively, although some authors assume bulk Ba nitrates where the outer layer is more reactive than Ba sites residing within the particle [3,27].

In order to account for the participation of Ba nitrates with different reactivity in the reduction with ammonia the energy of activation of step S5 was assumed to depend on the surface concentration of Ba-nitrates according to the following sigmoid function:

$$(E_{S5}) \quad E_{S5} = E_{MIN} + \frac{[E_{MAX} - E_{MIN}]}{[1 + \exp(\alpha(\Omega_{Ba(NO_3)}\theta_{Ba(NO_3)} - \gamma))]}$$

where E_{MIN} and E_{MAX} represent the minimum and maximum values of the energy of activation at the maximum and nil concentration

Table 5
Values of the parameter estimates for the reduction of stored NO_x with NH_3 and with H_2.

Step	Pre-exponential factor, k_4^0 (mol/m^{-3} s^{-1})		Activation energy, E_4 (kJ/mol)		
S4	3.45×10^6		22.94		
Step	k_5^0 (mol/m^3 s^1)	$E_{att\,MIN}$ (kJ/mol)	$E_{att\,MAX}$ (kJ/mol)	α	β
S5	1.26×10^{10}	116.7	138.0	0.1406	23.2

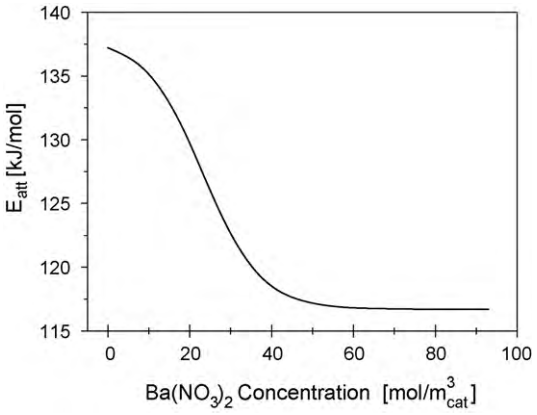

Fig. 2. Dependence of E_{att} of step S5 from $Ba(NO_3)_2$ concentration.

of $Ba(NO_3)_2$ respectively, α and γ are adaptive parameters that account for the slope and the position of the inflection point of the sigmoid curve.

The model predictions (full lines) and the experimental effluent concentrations at the MS detector (open symbols) are compared in Fig. 1. It is observed that the breakthrough time of NH_3 is predicted quite well by the model at any temperature; only at 200 °C the slope associated with the actual NH_3 concentration trace is somehow sharper and the breakthrough time is slightly longer than predicted by the model. The delay of the effluent ammonia concentration can be appreciated by comparing the concentration of ammonia predicted by the model at the MS detector (full lines) and at the reactor exit (dashed lines). At 150 °C the breakthrough of effluent ammonia, which here is due primarily to the time delay, disappears and at higher temperatures the concentration of ammonia at the reactor exit always anticipates that observed in the effluent stream at the MS and corresponds to the decrease in the concentration of nitrogen.

The values of the parameter estimates obtained by regression are reported in Table 3 for steps S1, S2 and S3, and in Table 5 for step S5. The dependence of E_{S5} from the surface concentration of $Ba(NO_3)_2$ is shown in Fig. 2. The energy of activation of step S5 is almost constant at the level of 117 kJ/mol from ca 93 mol $Ba(NO_3)_2/m^3_{cat}$ down to ca 60 mol $Ba(NO_3)_2/m^3_{cat}$, and then increases progressively up to 137 kJ/mol at mol $Ba(NO_3)_2/m^3_{cat}$ = 0. The change from 93 to 60 mol $Ba(NO_3)_2/m^3_{cat}$ corresponds to the consumption of ca 1×10^{-4} mol NO_x/g_{cat} that represents the amount of most reactive NO_x species.

From the physico-chemical characteristics of the catalyst it is possible to compute the quantity of NO_x species surrounding the Pt crystallites. Based on the mean dimension of the Pt crystallites given in Table 1 ($D_{Pt\,cryst}$ = 20 Å), the characteristics of the unit cell of Pt with the FCC structure (a_{Pt} = 3.9 Å; Z_{Pt} = 4) [JCPDS 4-802] and further assuming that the Pt crystallites have a hemispherical shape the number of Pt atoms per crystallite, $N_{Pt\,at}$/cryst, is obtained as:

$$\frac{N_{Pt\,at}}{cryst} = \frac{2}{3}\pi\left(\frac{D_{Pt\,cryst}}{2}\right)^3 \times \frac{1}{(a^3_{Pt})} Z_{Pt} = 141$$

The following number of Pt atoms per g of catalyst, $N_{Pt\,at}/g_{cat}$, is also calculated:

$$\frac{N_{Pt\,at}}{g_{cat}} = \left[\frac{x_{w\,Pt}}{M_{Pt}}\right] N_{Av} = 2.564 \times 10^{19}$$

Here $x_{w\,Pt}$ represents the catalyst weight fraction of Pt, M_{Pt} is the molecular weight of Pt, and N_{Av} is the Avogadro number. Next the number of crystallites per g of catalyst, $N_{Pt\,cryst}/g_{cat}$, is obtained using the following relation:

$$\frac{N_{Pt\,cryst}}{g_{cat}} = N_{Pt\,at}/g_{cat}/N_{Pt\,at}/cryst = 1.816 \times 10^{17}$$

and the total perimeter of Pt crystallites per g of catalyst, $P_{Pt\,cryst}/g_{cat}$, is calculated:

$$\frac{P_{Pt\,cryst}}{g_{cat}} = \pi D_{Pt\,cryst} \times \frac{N_{Pt\,cryst}}{g_{cat}} = 1.14 \times 10^{19}$$

Finally on the basis of the unit cell characteristics of $Ba(NO_3)_2$ with the FCC structure ($a_{(Ba(NO_3)_2)} = 8.12$ Å ; $Z_{(Ba(NO_3)_2)} = 4$) [JCPDS 24-53], and assuming that the Ba content ensures the complete coverage of the alumina surface in the catalyst the total number of moles of NO_x species per g of catalyst, that surround the Pt crystallites as first neighbours, N_{NOx}/g_{cat}, is obtained as follows:

$$\frac{N_{NO_x}}{g_{cat}} = P_{Pt\,cryst}/g_{cat}/a_{Ba(NO_3)_2} \times Z_{Ba(NO_3)_2} \times \frac{2}{N_{Av}} \times \frac{D_{Pt\,cryst} + a_{Ba(NO_3)_2}}{D_{Pt\,cryst}} = 2.64 \times 10^{-5}\ \text{mol}\ NO_x/g_{cat}$$

The assumption of a complete coverage of the alumina surface by BaO is in line with earlier findings by Castoldi et al. [6] and with the disappearance of the FTIR bands of alumina surface OH groups. The term $((D_{Pt\,cryst} + a_{(Ba(NO_3)_2)})/D_{Pt\,cryst}$ accounts for the geometrical coupling between the perimeter of the Pt crystallite and the unit cell of $Ba(NO_3)_2$. When the particle diameter distribution of the Pt crystallites is taken into account (e.g. 20 ± 5 Å) and the second neighbours to Pt crystallites are also considered, N_{NO_x}/g_{cat} becomes very close to the moles of the most reactive NO_x species provided by the kinetic study (near 1×10^{-4} mol/g_{cat}). This eventually confirms the association of the most reactive $Ba(NO_3)_2$ species, that are reduced by ammonia already at 150 °C, with those in close proximity to the Pt crystallites (i.e. first and second neighbours) and the association of the less reactive ones, that are reduced only at $T \geq 200$ °C, with those far from the Pt crystallites.

To explain the participation in the reduction process of less reactive $Ba(NO_3)_2$, i.e. of the species far from Pt, reverse spill-over of NO_x species on the surface of the $BaO/Ba(OH)_2$ phase and across the Pt-$BaO/Ba(OH)_2$ interface is likely involved, in line with previous literature indication [3,42,43]. in this case the role of the reductant is to keep Pt in a reduced state. It is noted that the reduction of stored NO_x does not occur to an appreciable extent over BaO/Al_2O_3 at any temperature [17] while NO_x stored far from Pt are effectively reduced at low temperature (150 °C) with H_2 (see below) but not with ammonia. Accordingly the nature of reducing agent does affect the reduction of metal sites and/or the mobility of the stored NO_x species. Still the involvement of hydrogen spillover (after activation of H_2 on Pt sites) toward nitrate adspecies cannot be excluded, although these aspects deserve further investigations.

The most reactive Ba sites in close proximity to Pt crystallites are regenerated at first during reduction but are saturated at first during NO_x storage as well. The less reactive Ba sites are involved later on after the most reactive sites have been either regenerated during reduction or occupied during NO_x storage. Indeed it has been shown that the most effective pathway for NO_x storage from NO/O_2 is represented by the stepwise oxidation of NO followed by adsorption at a Ba site in proximity of the Pt site leading to the formation of nitrite adsorbed species (nitrite route) [37]. Nitrites are then progressively transformed into nitrates that are predominant at catalyst saturation [37,44]. Oxidation of NO to NO_2 by gaseous oxygen can also occur; the NO_2 so formed can be stored on BaO either close to or far from the Pt site directly in the form of nitrates according to a disproportion reaction to give Ba-nitrates and NO (nitrate route): $3NO_2 + BaO \rightarrow Ba(NO_3)_2 + NO$. As nitrites are

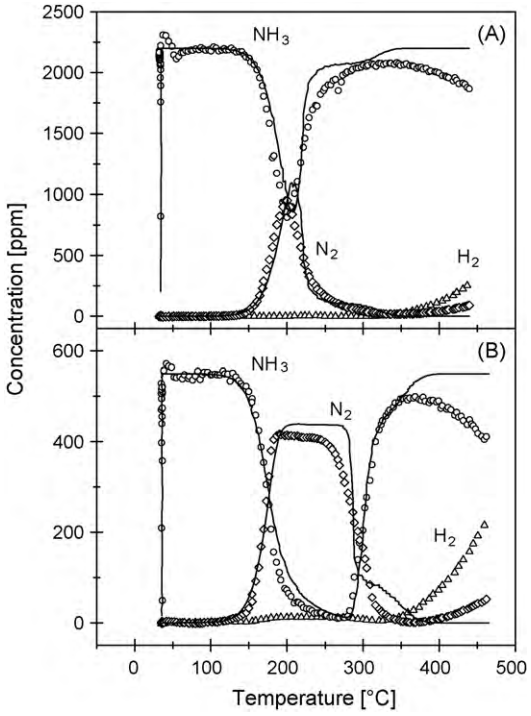

Fig. 3. NH_3-TPSR runs performed with 1% H_2O in the feed after NO_x adsorption at 350 °C: (A) 2200 ppm of NH_3; (B) 550 ppm of NH_3. Experimental effluent concentration of NH_3, N_2 and H_2 at the MS detector, open symbols; model prediction of effluent concentrations of NH_3, N_2 and H_2 at the MS detector, full lines.

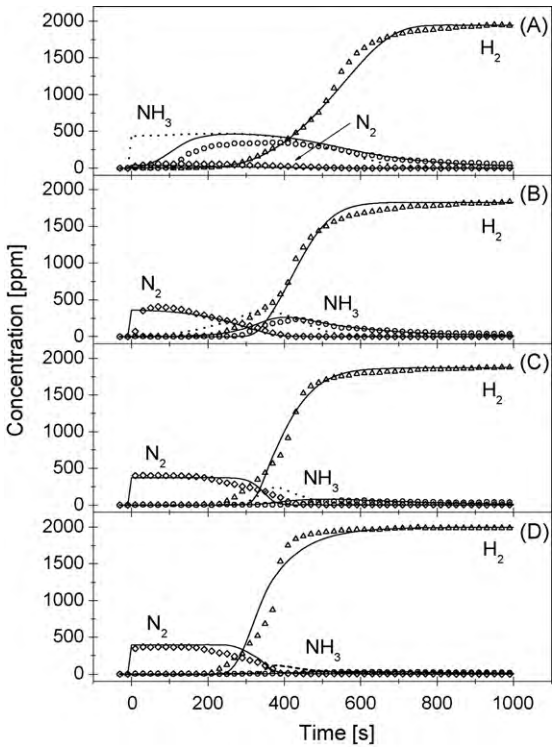

Fig. 4. Isothermal reduction with H_2 of NO_x stored at 350 °C: (A) T = 150 °C; (B) T = 200 °C; (C) T = 250 °C; (D) T = 350 °C. Experimental effluent concentration of H_2, NH_3 and N_2 at the MS detector, open symbols; model prediction of effluent concentration of H_2, NH_3 and N_2 at the MS detector, full lines; model prediction of effluent concentration of NH_3 at the reactor exit, dashed lines. The inlet concentration of H_2 is set at 1000 ppm at t = 0.

the most abundant species before NO_x breakthrough [37,44] and at low temperature [18] the nitrite pathway is believed to dominate over the nitrate pathway. It is noted that the nitrite route involves adsorption only at Ba sites in close proximity to the Pt crystallites while the nitrate route on the opposite can involve in principle Ba sites either close or far from the Pt crystallites. However since the former Ba sites have been already involved in the fast nitrite pathway the latter ones are believed to be preferentially involved in the nitrate route.

The model of the reduction of stored NO_x by NH_3 was validated without any adjustment of the parameter estimates by comparing experimental data collected during TPSR runs performed with 550 and 2200 ppm of NH_3 with 1% H_2O in the feed with model predictions (Fig. 3). The results shown in Fig. 3 demonstrate a very nice agreement between experimental data and model predictions. The apparent disagreement observed above 350 °C is due to ammonia decomposition into H_2 and N_2, which is not accounted for in the model.

3.2. Reduction of stored NO_x with H_2

The experiments where the reduction of NO_x stored at 350 °C was accomplished with hydrogen at 150, 200, 250 and 350 °C were used to estimate the parameters k_4^0 and E_4 while the parameters of step S5 and k^0_{des,NH_3} were fixed to the values given in Tables 3 and 5.

Fig. 4 shows the experimental concentration of effluent H_2 and of the effluent products (NH_3 and H_2) at the MS detector during the reduction of stored nitrates with hydrogen at different temperatures. At low temperature (150 °C in panel A) and at the beginning of the regeneration phase the consumption of hydrogen is complete and the reaction is controlled by the concentration of hydrogen, which indicates that hydrogen is more reactive than ammonia towards surface nitrates. Only NH_3 is observed among the products, which indicates that step S4 (reaction of nitrates with H_2 to give NH_3) is faster than step S5 (reaction of nitrates with NH_3 to give N_2). This is in line with the results in Fig. 1 showing only a very limited conversion of ammonia to nitrogen at the same temperature. Effluent NH_3 is detected with a large time delay due to NH_3 adsorption–desorption on the Mass Spec capillary. At 200 °C (panel B) immediately upon hydrogen admission the consumption of H_2 is complete, and only nitrogen is observed among the products. This is due to the fact that NH_3 produced through step S4 is consumed through step S5, which indeed at 200 °C is expectedly faster than at 150 °C. At higher regeneration times a decrease in the effluent nitrogen concentration is observed which again anticipates the increase in the concentration of effluent NH_3, due to ammonia adsorption–desorption onto the Mass Spec capillary line. The increase in effluent NH_3 concentration is observed in correspondence to the hydrogen breakthrough due to the ammonia time delay. At higher temperatures (i.e. 250 °C in panel C and 350 °C in panel D) the amount of effluent ammonia detected during the experiment is much smaller because the relative importance of the rate of ammonia consumption (step S5) as compared to that of ammonia production (step S4) increases with temperature, i.e. the process is less kinetically controlled by step S5 as the temperature increases. At these high temperatures ammonia is detected well after the hydrogen breakthrough.

From these experiments and the final reduction run accomplished thereafter at 350 °C it is possible to calculate for each temperature the moles of NO_x reduced by H_2 to form nitrogen (after the time period shown in Fig. 4 and till the end of the experiment) and also the sum of these moles with those that are reduced at 350 °C; these last ones correspond to those previously stored onto the catalyst at 350 °C. These quantities are listed in Table 4. In the same table the reduction efficiency at the end of the isothermal experiments, defined as the ratio between the moles of NO_x

reduced at a given temperature to the sum of these moles with those that are reduced thereafter at 350 °C, is also given. The NO_x reduction efficiency is close to 100% at any temperature. The comparison between the moles of NO_x consumed during the reduction with H_2 and with NH_3 at low temperatures (150 and 200 °C) confirms that step S4 is faster than step S5.

The values of the parameter estimates obtained by regression of the experimental data in Fig. 4 are shown in Table 5. The model predictions (full lines) and the experimental effluent concentrations (open symbols) are compared in Fig. 4. The concentration profiles of both products NH_3 and N_2 and the breakthrough time of the reagent H_2 are well predicted by the model at any temperature. In Fig. 4 the reaction is limited by the concentration of the reducing agent up to a consumption of about $1.5–2 \times 10^{-4}$ mol NO_x/g_{cat}. Accordingly, on the basis of the previous analysis of regeneration of stored NO_x with ammonia, the low activation energy estimated for the reduction of nitrates to NH_3 (22.94 kJ/mol) applies to residual NO_x species far from the Pt crystallites and the reaction is limited by the surface mobility of the stored NO_x species. Accordingly the use of the kinetic parameters for step S4 in Table 5 up to the consumption of about 1×10^{-4} mol NO_x/g_{cat}, that on the basis of the present study are associated to more reactive Ba sites close to Pt crystallites, is expected to underestimate the true rate of regeneration by hydrogen. Again the delay of the effluent ammonia concentration can be appreciated by comparing the concentration of ammonia predicted by the model at the MS detector (full lines) and at the reactor exit (dashed lines). At 150 °C in panel A the ammonia concentration at the reactor exit is high immediately after hydrogen admission while at the MS detector is predicted by the model only after 40 s. The breakthrough of ammonia at the reactor exit predicted by the

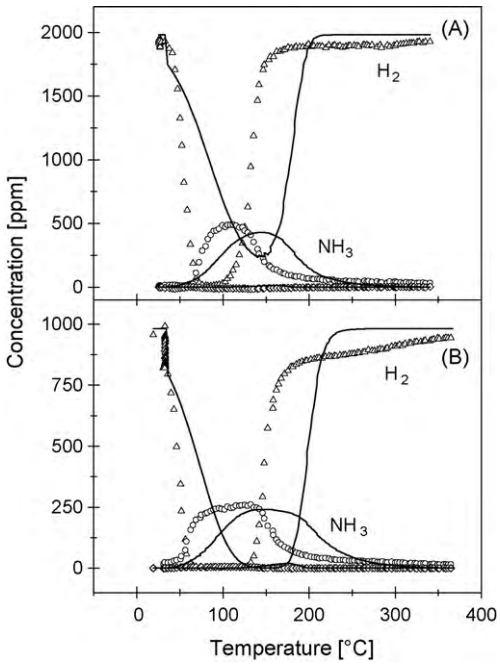

Fig. 5. H_2-TPSR runs performed with 1% H_2O in the feed after NO_x adsorption at 350 °C: (A) 2000 ppm of H_2; (B) 1000 ppm of H_2. Experimental effluent concentration of H_2, NH_3 and N_2 at the MS detector, open symbols; model prediction of effluent concentrations of H_2, NH_3 and N_2 at the MS detector, full lines.

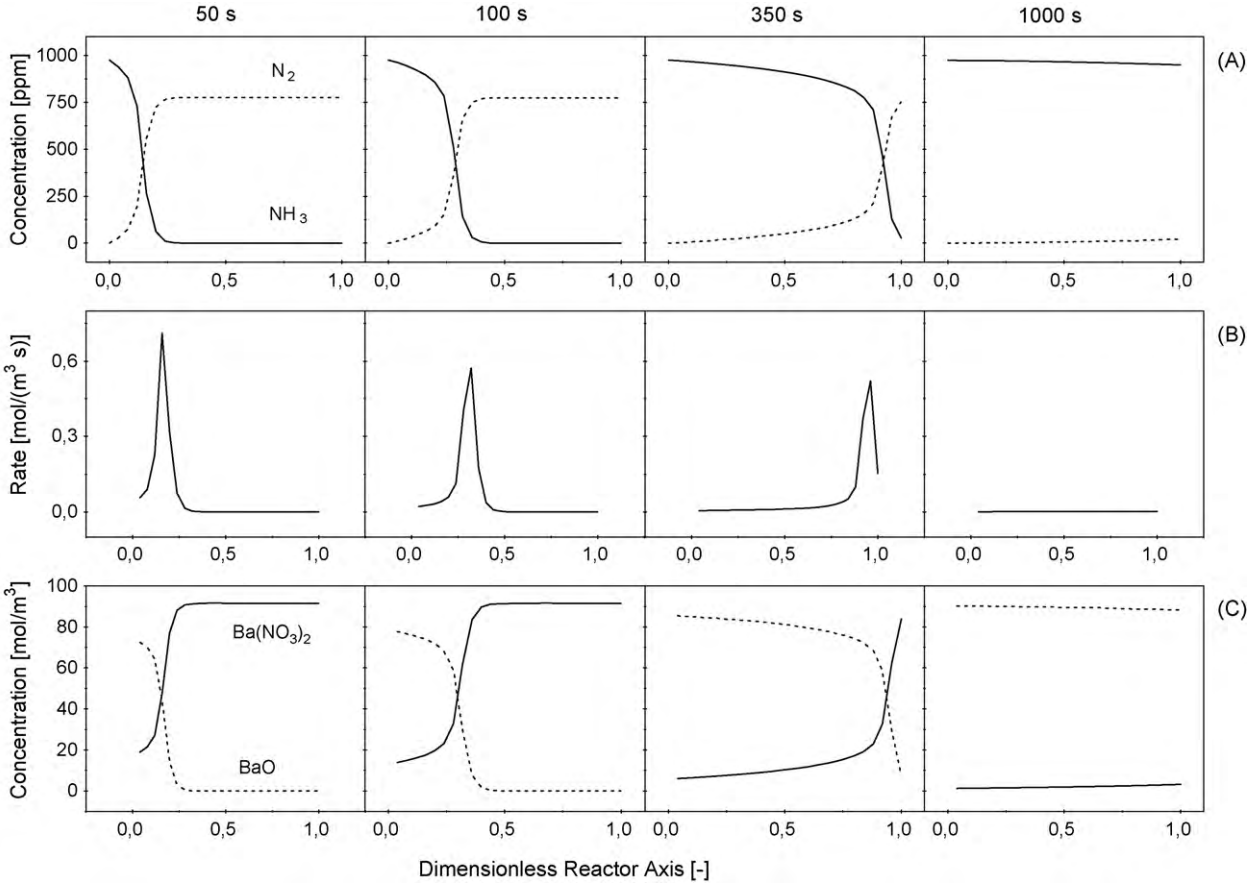

Fig. 6. Gas phase concentration of NH_3 (full line) and N_2 (dashed line) [panel A], rate of reduction of Ba-nitrate to give nitrogen [panel B] and surface concentration of $Ba(NO_3)_2$ (full line) and BaO (dashed line) [panel C] along the axial reactor coordinate at 300 °C at different regeneration times.

model (dashed lines) occurs before the H_2 breakthrough at 200 °C in panel B, together with the hydrogen breakthrough at 250 °C in panel C and after the hydrogen breakthrough at 350 °C in panel D. This behaviour originates from both the in series reaction scheme, where the reduction of nitrates by ammonia to give nitrogen follows the reduction of nitrates with hydrogen to give NH_3, and the integral behaviour of the reactor, that will be addressed later.

A validation of the kinetic model of the reduction of stored NO_x by H_2 was attempted by comparing experimental data collected during TPSR runs performed with 2000 and 1000 ppm of H_2 with 1% H_2O in the feed with model predictions without any adjustment of the parameter estimates. The results shown in Fig. 5 demonstrate that the model is able to capture the onset temperature of the reduction process and the formation of only ammonia among the products, but underestimates the consumption of hydrogen and the net production of ammonia at low T, i.e. below 100 °C. This is because the kinetic parameters in Table 5 apply only above a consumption of $1.5–2 \times 10^{-4}$ mol NO_x/g_{cat} where the residual stored NO_x are associated to less reactive Ba sites far from the Pt crystallites. Accordingly the model underestimates the true rate of regeneration of the more reactive Ba-nitrates close to the Pt crystallites that are reduced at first at low temperature.

3.3. Spatiotemporal resolution of LNT regeneration provided by the model

The model was used to simulate the axial concentration profiles in the reactor for gas and surface species as function of time during the reduction of stored NO_x with ammonia at different temperatures.

The gas phase concentration of NH_3 and N_2, the rate of reduction of Ba-nitrate to give nitrogen and the surface concentration of $Ba(NO_3)_2$ and BaO along the axial coordinate of the reactor at 300 °C are plotted at different times in Fig. 6. It is worth noting that the model prediction in Fig. 6 do not consider the ammonia delay that occurs downstream of the reactor in the MS capillary. NH_3 is consumed completely within a given length of the front part of the reactor and reaches a zero concentration downstream (panel A). The region where ammonia is consumed results in the production of N_2 (panel A); the reaction is confined in this region and the rate of reaction is limited by the concentration of the reducing agent to the value of ca 0.5–0.6 mol/m^3_{cat} s (panel B). The ammonia front moves towards the end of the reactor with time and the breakthrough is eventually observed at ca 350 s (dashed line in Fig. 1 panel D). N_2, the end product of the reduction process, is detected immediately at the exit of the reactor; it reaches the maximum concentration of 800 ppm immediately/after few seconds (about 10 s) and starts to decrease after the ammonia breakthrough (350 s). NH_3 is consumed at the expense of Ba-nitrates (panel C); its surface concentration at first decreases sharply to a non-nil residual value in a confined region of the reactor. As time goes on the $Ba(NO_3)_2$ consumption front moves towards the exit of the reactor, that is eventually reached at 350 s. In the meantime the residual surface concentration of $Ba(NO_3)_2$ left behind the consumption front decreases slowly and progressively: at the entrance of the reaction it decreases from 20 mol/m^3_{cat} at 50 s down to 6 mol/m^3_{cat} at 350 s and to 1.3 mol/m^3_{cat} at 1000 s. On the opposite the surface concentration of BaO increases in a parallel way because during reduction Ba-nitrates are transformed into BaO. As already noted BaO can be likely transformed into $Ba(OH)_2$ due to the presence of large amounts of water in the gas phase. The peculiar features of the $Ba(NO_3)_2$ consumption and of its dynamics as the regeneration proceeds is due to the presence of fast and slow regeneration sites that are described in the model by a coverage dependent energy of activation for step S5. The Ba-nitrates close to the metal crystallites react first and are responsible for the development of the $Ba(NO_3)_2$ consumption front while the Ba-nitrates far from the metal crystallites are left behind the consumption front and are consumed later on. Since the catalyst has been saturated during the previous storage phase both fast and slow storage/regeneration sites have been occupied at any axial position of the LNT reactor during storage and the amount of the fast sites according to the present kinetic study corresponds roughly to the value of 4×10^{-3} mol $Ba(NO_3)_2/m^3_{cat}$, i.e. 1×10^{-4} mol NO_x/g_{cat}.

At lower temperature (not shown) the rate of reaction is lower and the region where ammonia is consumed is larger. Also the ammonia breakthrough and the concomitant decline in the concentration of effluent nitrogen are observed earlier, namely at 300 s for T = 250 °C and at 10 s for T = 200 °C (see Fig. 1 panels C and B, respectively). At 250 °C a surface concentration front of $Ba(NO_3)_2$, that travels with time along the reactor axis, is still predicted by the model but is more smooth and the change with time of the residual concentration of $Ba(NO_3)_2$ left behind the concentration front is slower. At 200 °C the reaction rate is lower and the reaction is no longer confined in a portion of the reactor where it is limited by the concentration of the reducing agent. Accordingly a spatially confined concentration front of $Ba(NO_3)_2$ is no longer apparent and the axial profile of the concentration of $Ba(NO_3)_2$ develops along the entire length of the reactor. At 150 °C the axial profile of the gas and surface species are almost flat and a significant concentration of $Ba(NO_3)_2$ is still present after prolonged reaction time due to the very low rate of reaction.

The same spatiotemporal analysis was not attempted for the regeneration of stored NO_x with hydrogen, because the kinetic parameters estimated for step S4 in the present study are valid only after a consumption of $1.5–2 \times 10^{-4}$ mol NO_x/g_{cat} and the model underestimates the reactivity of fast regeneration sites.

4. Conclusions

A kinetic model based exclusively on a consecutive reaction scheme with ammonia as intermediate was developed which includes adsorption–desorption of hydrogen, ammonia and water at Pt site, the reduction of stored nitrates by hydrogen to give ammonia and the reduction of stored nitrates by ammonia to give nitrogen. The delay in the ammonia signal observed in the experiments was described by NH_3 adsorption–desorption occurring onto the Mass Spec capillary line in series to the catalytic reactor. The model was shown to capture the major features of the isothermal experiments performed over a Pt-BaO/Al_2O_3 catalyst with hydrogen and ammonia as reducing agents in the T interval 150–350 °C and under wet conditions.

The rate constants of adsorption–desorption of hydrogen, ammonia and water were taken from the literature (except the pre-exponential factor of ammonia desorption) while the other parameters were estimated by regression to the experiments. A surface dependent energy of activation was assumed for the reduction of stored nitrates by ammonia to give nitrogen in order to describe the data collected in the investigated temperature interval when ammonia was employed as the reducing agent. This is explained with the presence of nitrates with high and low reactivity that are envisaged as close or far from the noble metal crystallites, respectively. Besides a low energy of activation was estimated for the reduction of nitrates by hydrogen to give ammonia. This view applies for a consumption level of stored NO_x above $1.5–2 \times 10^{-4}$ mol NO_x/g_{cat}, where the NO_x species are expectedly stored far from the Pt crystallites, and the reaction is limited by surface diffusion. Below this consumption value the reaction is limited by the concentration of the reducing agent at any temperature.

The model was validated against independent NH_3- and H_2-TPSR data. A very nice agreement was obtained for the NH_3-TPSR

data but the model underestimated the consumption of hydrogen at high concentration of Ba-nitrates and at low temperature during H_2-TPSR. This is because the kinetic model underestimates the true rate of regeneration with hydrogen of the most reactive Ba-nitrates close to the Pt crystallites, that are reduced at first at low temperature.

The model was also used to simulate the axial concentration profiles in the reactor for gas and surface species as function of time during the regeneration of the LNT catalyst with ammonia. During regeneration an ammonia front develops which moves towards the end of the reactor and eventually breaks through while nitrogen, the end product of the reduction process, is detected immediately at the exit of the reactor, reaches the maximum concentration of 800 ppm after few seconds and decreases only after the ammonia breakthrough. Also a consumption front of Ba-nitrates develops which travels towards the end of the reactor and eventually it breaks through. The consumption front is associated with most reactive Ba-nitrates in close proximity to the Pt crystallites. In the same time a residual concentration of $Ba(NO_3)_2$, associated with less reactive nitrates stored far from the Pt crystallites, is left behind the consumption front, which decreases slowly and progressively with time.

The kinetic model developed in the present paper differs from those available in the literature because it considers the most relevant physico-chemical features of regeneration of LNT catalysts under nearly isothermal conditions. These include a mechanism based only on surface reaction of stored NO_x, a pathway consisting exclusively of a consecutive reaction scheme with ammonia as intermediate and the presence of slow and fast reduction sites associated with NO_x stored close and far from the noble metal crystallites, respectively.

References

[1] L. Lietti, I. Nova, P. Forzatti, Catal. J. 257 (2008) 270–282.
[2] N. Takahashi, H. Shinjoh, T. Iijima, T. Suzuki, K. Yamazaki, K. Yokota, H. Suzuki, N. Miyoshi, S. Matsumoto, T. Tanizawa, T. Tanaka, S. Tateishi, K. Kasahara, Catal. Today 27 (1996) 63–69.
[3] W.S. Epling, L.E. Campbell, A. Yezerets, N.W. Currier, J.E. Parks, Catal. Rev.: Sci. Eng. 46 (2004) 163–245.
[4] L. Lesage, C. Verrier, P. Bazin, J. Saussey, M. Daturi, Phys. Chem. Chem. Phys. 5 (2003) 4435–4440.
[5] L. Lesage, C. Verrier, P. Bazin, J. Saussey, S. Malo, C. Hedouin, G. Blanchard, M. Daturi, Top. Catal. 30–31 (2004) 31–36.
[6] L. Castoldi, I. Nova, L. Lietti, P. Forzatti, Catal. Today 96 (2004) 43–52.
[7] J. Parks, S. Huff, J. Phil, J.-S. Choi, B. West, SAE Technical Paper 2005-01-3876, 2005.
[8] J.A. Pihl, J.E. Parks, C.S. Daw, T.W. Root, SAE Technical Paper 2006-01-3441, 2006.
[9] I. Nova, L. Castoldi, L. Lietti, E. Tronconi, P. Forzatti, Top. Catal. 42–43 (2007) 21–25.
[10] I. Cumaranatunge, S.S. Mulla, A. Yezerets, N.W. Currier, W.N. Delgass, F.H. Ribeiro, J. Catal. 246 (2007) 29–34.
[11] S.S. Mulla, S.S. Chaugule, A. Yezerets, N.W. Currier, W.N. Delgass, F.H. Ribeiro, Catal. Today 136 (2008) 136–145.
[12] J.-S. Choi, W.P. Partridge, J.A. Pihl, C.S. Daw, Catal. Today 136 (2008) 173–182.
[13] I. Nova, L. Lietti, P. Forzatti, Catal. Today 136 (2008) 128–135.
[14] P. Forzatti, L. Lietti, I. Nova, Energy Environ. Sci. 1 (2008) 236–247.
[15] R.D. Clayton, M.P. Harold, V. Balakotaiah, Appl. Catal. B 84 (2008) 616–630.
[16] W.P. Partridge, J.-S. Choi, Appl. Catal. B. 91 (2009) 144–151.
[17] I. Nova, L. Lietti, L. Castoldi, E. Tronconi, P. Forzatti, J. Catal. 239 (2006) 244.
[18] P. Forzatti, L. Lietti, Catal. Today (2009), doi:10.1016/j.cattod.2008.11.023.
[19] H. Mazhoul, J.F. Brilhac, P. Gilot, Appl. Catal. B 20 (1999) 47–55.
[20] L. Olsson, H. Persson, E. Fridel, M. Skoglundh, B. Andersson, J. Phys. Chem. B 105 (2001) 196–209.
[21] L. Olsson, E. Fridel, M. Skoglundh, B. Andersson, Catal. Today 73 (2002) 263–270.
[22] A. Lindhom, N.W. Currier, J. Li, A. Yezerets, L. Olsson, J. Catal. 258 (2008) 273–288.
[23] J. Xu, R. Clayton, V. Balakotaiah, M. Harold, Appl. Catal. B 77 (2008) 395–408.
[24] R.S. Larson, J.A. Pihl, V.K. Chakravarthy, T.J. Toops, C.S. Daw, Catal. Today 136 (2008) 104–120.
[25] A. Guthenke, D. Chatterjee, M. Weibel, N. Waldbuβer, P. Koci, M. Marek, M. Kubicek, Chem. Eng. Sci. 62 (2007) 5357–5363.
[26] P. Koci, F. Plat, J. Stepanek, M. Kubicek, L. Marek, Catal. Today 137 (2008) 253–260.
[27] U. Tuttlies, V. Schmeisser, G. Eigenberger, Chem. Eng. Sci. 59 (2004) 4731–4738.
[28] L. Olsson, R.J. Blint, E. Fridell, Ind. Eng. Chem. Res. 44 (2005) 3021–3032.
[29] L. Olsson, D. Monroe, R. Blint, Ind. Eng. Chem. Res. 45 (2006) 8883–8890.
[30] M. Sharma, R. Clayton, M.P. Harold, V. Balakotaiah, Chem. Eng. Sci. 62 (2007) 5176–5181.
[31] M. Sharma, M.P. Harold, V. Balakotaiah, Ind. Eng. Chem. Res. 44 (2005) 6264–6277.
[32] C.M.L. Scholtz, V.R. Gangwal, M. de Croon, J.C. Shoulten, J. Catal. 245 (2007) 215–227.
[33] L. Cao, J.L. Ratts, A. Yezerets, N.W. Currier, J.M. Caruthers, F.H. Ribeiro, N.W. Delgass, Ind. Eng. Chem. Res. 47 (2008) 9006–9017.
[34] D. Bhatia, R.D. Clayton, M.P. Harold, V. Balakotaiah, Catal. Today 147S (2009) S250–S256.
[35] M. Boudard, G. Djéga-Mariadassou, Kinetics of Heterogeneous Catalytic Reactions, Princeton University Press, Princeton, NJ, 1984.
[36] F. Frola, M. Manzoli, F. Prinetto, G. Ghiotti, L. Castoldi, L. Lietti, J. Phys. Chem. C 112 (2008) 12869–12878.
[37] I. Nova, L. Castoldi, L. Lietti, E. Tronconi, P. Forzatti, F. Prinetto, G. Ghiotti, J. Catal. 222 (2004) 377–388.
[38] R. Rinnemo, O. Deutschmann, F. Behrendt, B. Kasemo, Comb. Flame 111 (4) (1997) 312–326.
[39] J.J. Vajo, W. Tsai, W.H. Weinberg, J. Phys. Chem. 89 (15) (1985) 3243–3251.
[40] G. Buzzi-Ferraris, F. Manenti, Interpolation and Regression Models for the Chemical Engineer Solving Numerical Problems, Wiley-VCH, Weinheim, Germany, 2009, ISBN: 978-3-527-32651-5.
[41] G. Buzzi-Ferraris, F. Manenti, Chem. Eng. Sci. 64 (2009) 1061–1074.
[42] G. Zhou, L.T. Lou, R.J. Gorte, Appl. Catal. B 64 (2006) 88–95.
[43] N.W. Cant, I.O.Y. Liu, M.J. Patterson, Catal. J. 243 (2006) 309–317.
[44] I. Nova, L. Castoldi, F. Prinetto, V. Dal Santo, L. Lietti, E. Tronconi, P. Forzatti, G. Ghiotti, R. Psaro, S. Recchia, Top. Catal. 52 (2009) 1757–1761.